Biochemistry

 Volume 40, Number 51 December 25, 2001

## Accelerated Publications

# Structure and Dynamics of Hydrated Statherin on Hydroxyapatite As Determined by Solid-State NMR†

Joanna R. Long,‡,§,|| Wendy J. Shaw,‡,||,⊥ Patrick S. Stayton,*,§ and Gary P. Drobny*,‡

*Department of Chemistry and Department of Bioengineering, University of Washington, Seattle, Washington 98195*

*Received April 27, 2001; Revised Manuscript Received July 17, 2001*

ABSTRACT: Proteins directly control the nucleation and growth of biominerals, but the details of molecular recognition at the protein−biomineral interface remain poorly understood. The elucidation of recognition mechanisms at this interface may provide design principles for advanced materials development in medical and ceramic composite technologies. Here, we have used solid-state NMR techniques to provide the first high-resolution structural and dynamic characterization of a hydrated biomineralization protein, salivary statherin, adsorbed to its biologically relevant hydroxyapatite (HAP) surface. Backbone secondary structure for the N-terminal dodecyl region was determined using a combination of homonuclear and heteronuclear dipolar recoupling techniques. Both sets of experiments indicate the N-terminus is α-helical in character with the residues directly binding to the HAP being stabilized in the α-helical conformation by the presence of water. Dynamic NMR studies demonstrate that the highly anionic N-terminus is strongly adsorbed and immobilized on the HAP surface, while the middle and C-terminal regions of this domain are mobile and thus weakly interacting with the mineral surface. The direct binding footprint of statherin is thus localized to the negatively charged N-terminal pentapeptide sequence. Study of a site-directed mutant demonstrated that alteration of the only anionic side chain outside of this domain did not affect the dynamics of statherin on the HAP surface, suggesting that it does not play an important role in HAP binding.

The construction of impressive inorganic structures is developmentally controlled in organisms ranging from marine coccoliths to higher vertebrates (*1*). The remarkable material properties of hard tissues thus result from the activities of a number of proteins that function at the organic−inorganic interface (*2*−*4*). A better understanding of how these proteins recognize and assemble in bioactive fashion on inorganic mineral phases should provide key insight into biological materials processing strategies and may aid in the development of surface modification approaches for biomaterials. Many of the proteins directly involved in control of biomineral nucleation and growth contain acidic domains that are rich in aspartic acid and glutamic acid and phosphorylated serines (*2*, *5*). To gain insight into how these acidic domains recognize hydroxyapatite, the principal mineral phase of bone and teeth, we have been studying statherin, a particularly well studied acidic phosphoprotein found in saliva. Statherin functions biologically to inhibit the nucleation and growth of calcium phosphate minerals,

† Funding provided by the National Dental Institute (Grant DE 12554), the National Science Foundation (Grants DMR-9616212 and EEC-9529161), and the Department of Energy through Associated Western Universities (W.J.S.).

* To whom correspondence should be addressed. G.P.D.: Department of Chemistry, Box 351700, University of Washington, Seattle, WA 98195; phone, (206) 685-2052; fax, (206) 685-8665; e-mail, drobny@macmail.chem.washington.edu. P.S.S.: Department of Bioengineering, Box 352125, University of Washington, Seattle, WA 98195; phone, (206) 685-8148; fax, (206) 685-8256; e-mail, stayton@u.washington.edu.

‡ Department of Chemistry.

§ Department of Bioengineering.

|| These authors contributed equally to this work.

⊥ Present address: Battelle Northwest, 908 Battelle Blvd., Richland, WA 99352.

10.1021/bi010864c CCC: $20.00 
Published on Web 11/28/2001

and also acts as a boundary lubricant (*5*−*10*). The N-terminus of statherin is highly charged, with the first five amino acids being one aspartic acid, two phosphorylated serines, and two glutamic acids that have been shown to be important in the recognition of HAP[1] (*6*).

Recent solid-state NMR experiments have been carried out on N-terminal statherin peptide fragments adsorbed to the HAP surface and lyophilized (*11*, *12*). These determined the acidic residues to be in an extended conformation and residues 7−12 to be partly helical. Site-specific isotopic labeling of peptides and proteins allows molecular structure determinations to be made unambiguously using the dipolar recoupling techniques DRAWS, DQDRAWS, and REDOR (*13*−*15*). DRAWS and DQDRAWS, a double-quantum variant of the DRAWS homonuclear recoupling technique, can be used to measure the distance between adjacent backbone carbonyl carbons and thus yield a model-free determination of the backbone torsion angle $\varphi$. Determination of individual torsion angles yields insights into local secondary structure as well as structural heterogeneity. Typical α- and $3_{10}$-helices are characterized by $\varphi$ torsion angle values in the range of −45° to −80°, with a mean of −63°. The average values of $\beta$-sheets are somewhat larger, varying from −80° to −150° with a mean of −130° (*16*). Although isotropic chemical shifts of proteins can give qualitative indications of secondary structure in homogeneous systems, their values can be influenced by the bulk magnetic susceptibility of the support in heterogeneous systems. This makes them unreliable for structural determination in proteins closely associated with or adsorbed on inorganic surfaces such as HAP (*17*).

Complementary and confirmatory structural data can be obtained with REDOR, a heteronuclear recoupling technique, which provides a measurement of the distance between the backbone carbonyl carbon and the backbone nitrogen involved in the hydrogen bond of the putative α-helical domain (i.e., $i$ to $i + 4$ positions). This measurement is very sensitive to global secondary structure since theoretical distances expected for classical secondary structures vary from 4.2 Å for an α-helix to 5.2 Å for a $3_{10}$-helix to 10.6 Å for a $\beta$-sheet (*15*). Solid-state NMR of $^{13}$C nuclei is also very sensitive to dynamics, (*18*) which can be probed over several orders of magnitude by measuring chemical shift anisotropies (CSAs) (*19*), relaxation constants (*20*), and cross polarization efficiencies (*18*). This suite of solid-state NMR techniques has been applied here to full-length phosphorylated statherin on the HAP crystal surface to characterize the high-resolution structure and dynamics of the N-terminal binding domain under hydrated and lyophilized conditions. The results provide insight into the molecular structure−function relationships that define statherin recognition of HAP and suggest that the interaction mechanism is tied to important dynamic properties.

## METHODS

*Sample Preparation*. Isotopically enriched amino acids were protected and incorporated during synthesis of the protein using standard Fmoc solid-phase peptide synthesis strategies. Phosphorylated serine was incorporated into the protein during synthesis in most cases; for the serine $^{13}$C═O-enriched samples, phosphorylation was accomplished after synthesis. The samples were purified using HPLC, and purity was verified using electrospray mass spectroscopy with a single species observed at 5381 ± 2. Adsorption to 80 m$^2$/g of HAP and preparation of the NMR samples were carried out as previously described (*11*) using an initial solution statherin concentration of 40 $\mu$M. NMR samples contained 100 mg of HAP with approximately 1−3 $\mu$mol of adsorbed protein.

*NMR Spectra*. CPMAS spectra were acquired at room temperature on a home-built 500 MHz spectrometer using spinning speeds of 3, 4, and 5 kHz. Cross polarization was accomplished with a 2 ms contact time at RF fields of 50 kHz, and data were collected during 100 kHz proton decoupling. $T_{1\rho}$ measurements were taken at a spinning speed of 6 kHz on a Chemagnetics Infinity 300 instrument using $^{13}$C spin lock times of 0.05−4.55 ms at an RF field of 42 kHz after cross polarization for 1.5 ms with 70 kHz proton decoupling during acquisition. REDOR measurements were carried out on a Chemagnetics Infinity 300 spectrometer using a spinning speed of 4 kHz, a 43 kHz $^{13}$C RF field, a 45 kHz $^{15}$N RF field, XY8 phase cycling on both channels, and 70 kHz decoupling. Measurements on the hydrated samples were carried out at −25 °C to remove any motions on the time scale of the REDOR experiment (as verified by $T_{1\rho}$ relaxation measurements). DQDRAWS data were taken at room temperature on a 500 MHz home-built spectrometer using a 4 kHz spinning speed, a 34 kHz $^{13}$C RF field, and 100 kHz proton decoupling.

*Simulations*. CSAs were determined by modeling the observed isotropic and side-band intensities at the three different spinning speeds. $T_{1\rho}$ data were fit using a simple exponential decay. DQDRAWS buildup and REDOR dephasing curves were simulated using C++ code operating in a Matlab environment. Simulations incorporated the observed CSAs, experimental parameters, principal axes of the CSAs relative to the amide bonds (molecular frame), and independently measured relaxation parameters.

## RESULTS AND DISCUSSION

The structure and dynamics of salivary statherin were analyzed at the $pS_2$, $pS_3$, $F_7$, $L_8$, $I_{11}$, and $G_{12}$ residues (see Table 1 for the primary sequence). Pairs of backbone carbonyl carbons were enriched at the $pS_2pS_3$, $F_7L_8$, and $I_{11}G_{12}$ positions in separate samples and probed using DRAWS and DQDRAWS. A $^{13}$C-enriched carbonyl carbon was introduced at position $i$ with a $^{15}$N-enriched amide nitrogen at position $i + 4$ in the $pS_3F_7$ and $L_8G_{12}$ samples and probed using REDOR to verify the presence or absence of hydrogen bonding. The dipolar recoupling data for the $pS_2pS_3$ and $pS_3F_7$ samples are shown in Figure 1. All five samples were characterized using standard $^{13}$C CPMAS and $T_{1\rho}$ relaxation sequences to measure any averaging of carbonyl carbon CSAs, cross polarization efficiencies, or relaxation due to the presence of motion. Measurements on all samples were performed under buffered, hydrated conditions as well as after lyophilization. These results are summarized in Table 1.

[1] Abbreviations: NMR, nuclear magnetic resonance; HAP, hydroxyapatite; DRAWS, dipolar recoupling with a windowless sequence; DQDRAWS, double-quantum dipolar recoupling with a windowless sequence; REDOR, rotational echo double resonance; CSA, chemical shift anisotropy; RF, radiofrequency.

Table 1: Values for the Anisotropy ($\Delta\sigma$) and Assymmetry ($\eta$) of the CSA, Average Values of the Torsion Angle ($\varphi$), Distance Measurements across Putative Hydrogen Bonds, and $^{13}C$ $T_{1\rho}$ Relaxation Constants Measured for the Indicated Residues of Salivary Statherin Bound to HAP in the Presence and Absence of Water

| DpSpSEEKFLRRIGRFGYGYGPYQPVPEQPLYPQPYQPQYQQYTF | | | | | | | | |
|---|---|---|---|---|---|---|---|---|
| | $\Delta\sigma^a$ (ppm) | | $\eta^b$ | | $\varphi$ or distance$^c$ | | $T_{1\rho}$ (ms) | |
| isotopic label | lyo | hydr | lyo | hydr | lyo | hydr | lyo | hydr |
| $pS_2$ | 114 | 105 | 0.96 | 0.74 | | | >20 | 18.2 |
| $pS_3$ | 109 | 104 | 0.81 | 0.79 | $-85° \pm 11°$ | $-60° \pm 10°$ | | |
| $pS_3F_7$ | | | | | 5.2 ± 0.6 Å | 4.3 ± 0.2 Å | | |
| $F_7$ | 103 | 99 | 0.73 | 0.61 | | | >20 | 7.5 |
| $L_8$ | 103 | 98 | 0.72 | 0.69 | $-77° \pm 20°$ | | | |
| $L_8G_{12}$ | | | | | 4.8 ± 0.4 Å | 4.8 ± 0.4 Å | | |
| $I_{11}G_{12}$ | 103 | 103 | 0.75 | 0.83 | $-65° \pm 13°$ | | >20 | 2.5 |

[a] $\Delta\sigma = \sigma_{33} - (\sigma_{22} + \sigma_{11})/2$. [b] $\eta = |(\sigma_{22} - \sigma_{11})/\sigma_{33}|$, where $\sigma_{33} > \sigma_{22} > \sigma_{11}$ and $\sigma_{33} + \sigma_{22} + \sigma_{11} = 0$. Values are reported in significant digits. [c] Limits where $\sigma = 1$ indicated.

Both the single torsion angle measurements on room-temperature samples and the distances between putative hydrogen bond donors and acceptors in frozen samples indicate the N-terminal 12 residues in statherin are in a helical conformation when adsorbed to HAP under biologically relevant conditions. REDOR measurements indicate the first six residues form an α-helix. The next six residues are also helical, but the slightly longer distance across the hydrogen bond between the $L_8$ and $G_{12}$ residues suggests minor populations of $3_{10}$-helix or more extended conformations. Removal of water via lyophilization under low vacuum (100 mT) results in a loss of this structure in the six highly acidic N-terminal residues. The extension of the helix during lyophilization suggests a significant role for water in stabilizing the binding domain (*21*). Water may mediate the interaction of the acidic side chains with the HAP surface or may be necessary for stabilizing the α-helix conformation. The α-helix has been previously suggested as a general structural mechanism for aligning acidic side chain residues with HAP (*6*), either through lattice matching or through more general electrostatic complementarity. Our data are consistent with this hypothesis and further point to the possible importance of bridging water in protein−HAP recognition.

The dynamic properties of the immobilized protein are a critical aspect of molecular recognition at the protein−biomineral interface, and relatedly to the function of proteins once adsorbed. Measurements of the dynamic properties of statherin in the presence and absence of water provide striking evidence that the direct binding footprint is largely confined to the acidic residues at the N-terminal pentapeptide region. The $^{13}C$ $T_{1\rho}$ values remain largely unchanged for the phosphoserines, indicating little or no motion is present in both the lyophilized and hydrated states. However, the $T_{1\rho}$ relaxation constants are considerably shorter in the hydrated samples at the $F_7$, $L_8$, $I_{11}$, and $G_{12}$ positions, indicating motion on the kilohertz time scale when water is present. Figure 2 shows each of the doubly carbon-labeled statherin samples under hydrated conditions, normalized to the natural abundance methyl region to account for any differences in the amounts of bound protein. A representative spectrum of a lyophilized, surface-bound sample labeled at the $pS_2$ and $pS_3$ positions is also shown for comparison.

The significant loss in CP efficiency at the $F_7$, $L_8$, $I_{11}$, and $G_{12}$ positions in the hydrated samples is also characteristic of mobility. These measurements bracket the time scale of the motion in this region to $10^{-3}$−$10^{-5}$ s. In contrast, the hydrated, surface-bound $pS_2pS_3$ region does not display a loss in CP efficiency, indicating there is very little motion in that region on the time scale of the cross polarization experiment. The CSAs are also sensitive to motion and were found to narrow very little for all of the samples, with anisotropies [$\Delta\sigma = \sigma_{33} - (\sigma_{22} + \sigma_{11})/2$] of approximately 98−105 ppm in the hydrated samples, as compared to 103−114 ppm for their lyophilized counterparts. The small change in the carbonyl carbon CSAs under hydrated conditions indicates that the motion observed in the cross polarization experiments, and supported by the $T_{1\rho}$ relaxation measurements, is somewhat restricted.

It is interesting to compare the dynamics of this N-terminal binding domain within the context of the whole statherin protein on HAP to the dynamics of the isolated peptide on HAP. Motion was observed in analogous regions for the SN15 peptide (*17*), but significant narrowing of the CSA was observed at the C-terminal residues of the peptide ($I_{11}$ and $G_{12}$). The nearly unchanging CSA observed for the N-terminus in statherin indicates that a different motional mode dominates the relaxation within the full protein. The $T_{1\rho}$ relaxation parameters for both the protein and peptide are nearly the same, which would support a motion of similar frequency in statherin, but with an amplitude different from that observed in the SN15 peptide. The change in mobility could be due to one of several factors, including motional limitations due to the larger size of the protein, stabilization of the protein backbone by tertiary structure, interactions between adsorbed protein molecules, or more substantial protein interactions with the surface at the C-terminal end of full-length statherin.

To explore the latter possibility, the only negatively charged residue outside of the N-terminus was replaced with its uncharged counterpart ($E_{26} \rightarrow Q_{26}$). This site-directed statherin mutant displayed a $T_{1\rho}$ value for the $I_{11}G_{12}$ sequence of 2.9 ms, identical within experimental uncertainty to the $T_{1\rho}$ value for the same positions of the unmodified protein (2.5 ms). This indicates that $Glu_{26}$ is not involved in HAP recognition to an extent that prevents kilohertz frequency motions in the N-terminal region. The simplest explanation of the dynamics results is that tertiary structural interactions tie the larger structure of the protein to the observed positions in the N-terminal domain, thus causing the lower-amplitude dynamics relative to those of the isolated SN15 peptide. However, current dynamics data do not rule out more

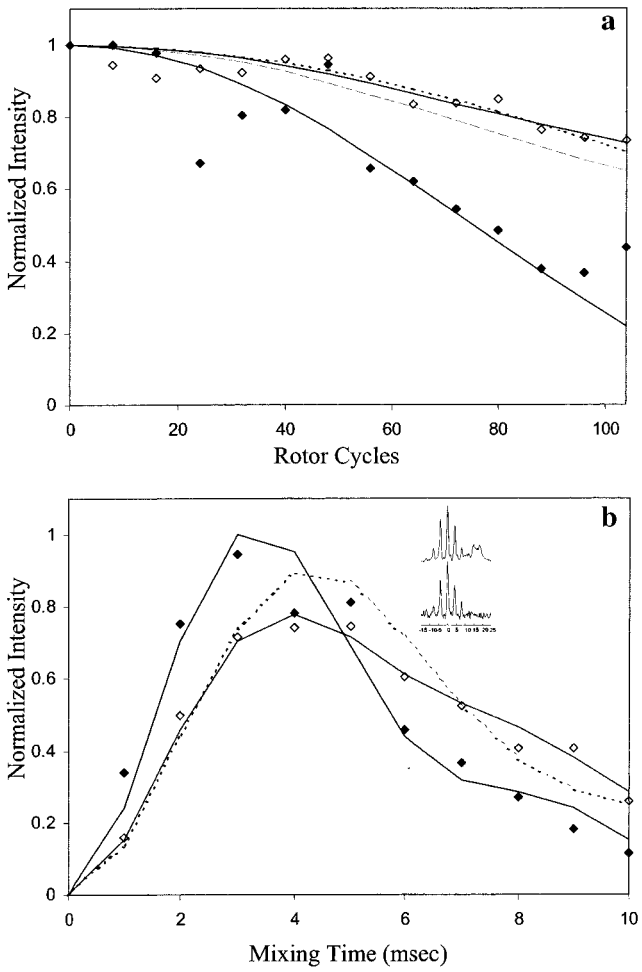


FIGURE 1: (a) REDOR dephasing curves for hydrated, surface-adsorbed $pS_3F_7$ statherin (◆) and lyophilized, bound $pS_3F_7$ statherin (◇) and simulations for 4.2 (—) and 5.2 Å (- - -) and a combination of 45% α-helix (4.2 Å) and 65% $\beta$-sheet (>8 Å) (— — —). The hydrated $pS_3F_7$ distance across the hydrogen bond fits best to a distance of 4.3 Å, indicating that the region is described well by an ideal α-helix. Data for the lyophilized sample are best simulated by 5.2 Å or a combination of 35% α-helix and 65% $\beta$-sheet, indicating a loss in α-helical secondary structure upon lyophilization. (b) DQDRAWS buildup curves for hydrated, surface-adsorbed $pS_2pS_3$ statherin (◆) and lyophilized, bound $pS_2pS_3$ statherin (◇) and simulations for $\phi$ torsion angles of −60° (—) and −85° (- - -) and a combination of 45% α-helix (−57°) and 65% $\beta$-sheet (−120°) (— — —). The increase in torsion angle on lyophilization correlates well with the loss of α-helical secondary structure. The inset demonstrates the selection of only the pair of isotopically enriched carbonyl carbons by the DQDRAWS experiment (bottom) in contrast to the significant contribution from natural abundance carbon observed in the CPMAS spectrum (top).

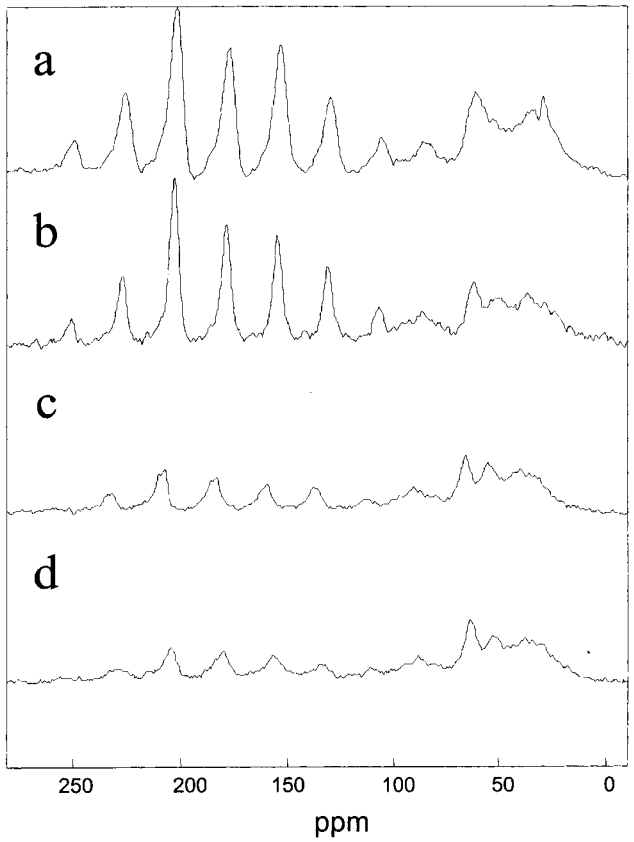


FIGURE 2: CPMAS spectra of (a) $pS_2pS_3$ statherin bound to the surface and lyophilized, (b) hydrated, surface-adsorbed $pS_2pS_3$ statherin, (c) hydrated, surface-adsorbed $F_7L_8$ statherin, and (d) hydrated, surface-adsorbed $I_{11}G_{12}$ statherin. Each hydrated spectrum is normalized to the natural abundance methyl region. The significant decrease in the carbonyl signal for the $F_7L_8$ and $I_{11}G_{12}$ hydrated spectra is indicative of molecular motion. $T_{1\rho}$ relaxation measurements support the interpretation of minimal mobility at the $pS_2pS_3$ region and increased mobility for the $F_7L_8$ and $I_{11}G_{12}$ regions.

complicated models that do include protein interactions with the surface outside of the N-terminal domain. It is clear, nonetheless, that both the full-length protein and N-terminal peptide fragments are only loosely associating with HAP outside of the anionic N-terminal pentapeptide region. This statherin pentapeptide sequence is a common motif in many bone- and tooth-associated proteins, and is also a recognition sequence for phosphorylation. The important role of the statherin-phosphorylated serines in binding to HAP is consistent with the use of phosphorylation as a regulatory mechanism in multifunctional proteins, such as osteopontin, which also contain this motif (*22*).

A molecular model consistent with the current structural and dynamic studies is shown in Figure 3. The N-terminal domain of residues 2−12 is helical on the surface. The strong interaction of statherin with HAP is mediated by the acidic N-terminus, where two phosphoserines and three carboxylate-containing side chains are located. The dynamics studies suggest that the remainder of the helix interacts much more weakly with HAP. The more weakly interacting residues in this domain can be viewed as a flexible rod, with torsional motions increasing with an increasing distance from the highly immobile N-terminal pentapeptide sequence. The presence of a highly mobile statherin segment could explain functional observations made previously by others in the field. Moreno et al. (*23*) found that statherin inhibited secondary crystal growth at surface coverages that were lower than expected on the basis of the theoretical surface area of the fixed, globular protein. The mobility of statherin on the surface could allow it to effectively block more nucleation sites than a very rigidly bound protein. The dynamic nature of statherin on the surface may also play a significant role in the lubricating properties of the protein. To adequately model the observed motions at the molecular level, further details of the surface-bound tertiary structure and experimental elucidation of the side chain interactions with HAP will be required to orient statherin at the surface.

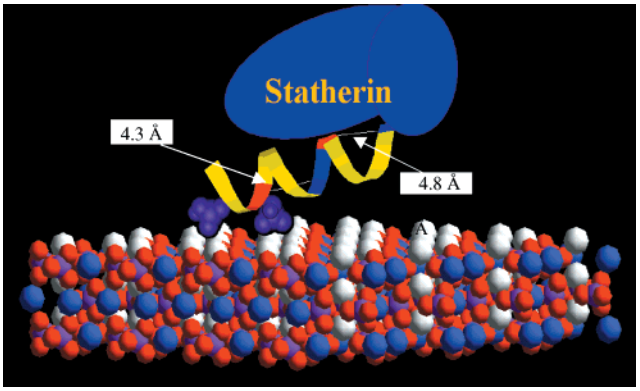


FIGURE 3: Schematic model showing statherin interacting with the 001 face of HAP, with calcium ions in white and phosphoserines in purple. The protein colors represent backbone $^{13}C{=}O$-enriched (red), $^{15}N$-enriched (blue), and unenriched (yellow) residues. The REDOR-measured hydrogen bonding distances are indicated for the hydrated N-terminal binding domain, while the remaining portion of the protein (blue) is shown as a nondescript shape to indicate unknown surface-adsorbed structure (hydrogen bonds in white). The strong interaction of the N-terminus through the immobile phosphoserines is indicated, and the more mobile, noninteracting C-terminus of the pentadecyl domain is shown oriented away from the HAP surface.

Solid-state NMR does provide a direct route to this information, and we are currently probing the tertiary structure and the interactions of side chains with the surface to further elucidate binding mechanisms.

## ACKNOWLEDGMENT

Special thanks to Nathan Oyler for the simulation code and Allison Campbell for HAP characterization. Some of the NMR experiments were performed at Battelle, Pacific Northwest National Laboratory, at the Environmental Molecular Sciences Laboratory (a national scientific user facility sponsored by the DOE Office of Biological and Environmental Research), operated by Battelle for the DOE.

## REFERENCES

1. Weiner, S., and Addadi, L. (1997) Design strategies in mineralized biological materials, *J. Mater. Chem. 7*, 689−702.
2. Hunter, G. K., and Goldberg, H. A. (1994) Modulation of crystal formation by bone phosphoproteins: role of glutamic acid-rich sequences in the nucleation of hydroxyapatite by bone sialoprotein, *Biochem. J. 302*, 175−179.
3. Hunter, G. K., Hauschka, P. V., Poole, A. R., Rosenberg, L. C., and Goldberg, H. A. (1996) Nucleation and inhibition of hydroxyapatite formation by mineralized tissue proteins, *Biochem. J. 317*, 59−64.
4. Fuijisawa, R., and Kuboki, Y. (1998) Conformation of dentin phosphophoryn adsorbed on hydroxyapatite crystals, *Eur. J. Oral Sci. 106*, 249−253.
5. Schlesinger, D. H., and Hay, D. I. (1977) Complete covalent structure of statherin, a tyrosine-rich acidic peptide which inhibits calcium phosphate precipitation from human parotid saliva, *J. Biol. Chem. 252*, 1689−1695.
6. Raj, P. A., Johnsson, M., Levine, M. J., and Nancollas, G. H. (1992) Dependence on sequence, charge, hydrogen bonding potency, and helical conformation for adsorption to hydroxyapatite and inhibition of mineralization, *J. Biol. Chem. 267*, 5968−5976.
7. Schwartz, S. S., Hay, D. I., and Schluckebier, S. K. (1992) Inhibition of calcium phosphate precipitation by human salivary statherin: structure−activity relationships, *Calcif. Tissue Int. 50*, 511−517.
8. Ramasubbu, N., Thomas, L. M., Bhandary, K. K., and Levine, M. J. (1993) Structural characteristics of human salivary statherin: a model for boundary lubrication at the enamel surface, *Crit. Rev. Oral Biol. Med. 4*, 363−370.
9. Gururaja, T. L., and Levine, M. J. (1996) Solid-phase synthesis and characterization of human salivary statherin: a tyrosine-rich phosphoprotein inhibitor of calcium phosphate precipitation, *Pept. Res. 9*, 283−289.
10. Naganagowda, G. A., Gururaja, T. L., and Levine, M. J. (1998) Delineation of conformational preferences in human salivary statherin by $^{1}H$, $^{31}P$ NMR and CD studies: sequential assignment and structure−function correlations, *J. Biomol. Struct. Dyn. 16*, 91−107.
11. Shaw, W. J., et al. (2000) Determination of statherin N-terminal peptide conformation on hydroxyapatite crystals, *J. Am. Chem. Soc. 122*, 1709−1716.
12. Long, J. R., et al. (1998) A peptide that inhibits hydroxyapatite growth is primarily in an extended conformation on the crystal surface, *Proc. Natl. Acad. Sci. U.S.A. 95*, 12083−12087.
13. Gregory, D. M., Wolfe, G. M., Jarvie, T. P., Sheils, J. C., and Drobny, G. P. (1996) Double-quantum filtering in magic-angle spinning NMR spectroscopy applied to DNA oligomers, *Mol. Phys. 89*, 1835−1849.
14. Gullion, T., and Schaefer, J. (1989) Rotational-echo double-resonance NMR, *J. Magn. Reson. 81*, 196−200.
15. Marshall, G. R., et al. (1990) Determination of precise interatomic distance in a helical peptide by REDOR NMR, *J. Am. Chem. Soc 112*, 963−964.
16. Smith, L. J., et al. (1996) Analysis of main chain torsion angles in proteins: prediction of NMR coupling constants for native and random coil conformations, *J. Mol. Biol. 255*, 494−506.
17. Shaw, W. J., Long, J. R., Campbell, A. A., Stayton, P. S., and Drobny, G. P. (2000) A solid-state NMR study of dynamics in a hydrated salivary peptide adsorbed to hydroxyapatite, *J. Am. Chem. Soc 122*, 7118−7119.
18. Mehring, M. (1983) *Principles of High-Resolution NMR in Solids*, Springer-Verlag, New York.
19. Herzfeld, J., and Berger, A. E. (1980) Sideband intensities in NMR spectra of samples spinning at the magic angle, *J. Chem. Phys. 73*, 6021−6030.
20. Schaefer, J., Stejskal, E. O., and Buchdahl, R. (1977) Magic-angle $^{13}C$ NMR analysis of motion in solid glassy polymers, *Macromolecules 10*, 384−405.
21. Kennedy, S. D., and Bryant, R. G. (1990) Structural effects of hydration: studies of lysozyme by $^{13}C$ solids NMR, *Biopolymers 29*, 1801−1806.
22. Jono, S., Peinado, C., and Giachelli, C. M. (2000) Phosphorylation of osteopontin is required for inhibition of vascular smooth muscle cell calcification, *J. Biol. Chem. 275*, 20197−20203.
23. Moreno, E. C., Varughese, K., and Hay, D. I. (1979) Effect of human salivary proteins on the precipitation kinetics of calcium phosphate, *Calcif. Tissue Int. 28*, 7−16.

BI010864C